JOURNAL OF GEOPHYSICAL RESEARCH, VOL. 114, A00C25, doi:10.1029/2008JA013519, 2009

THEMIS observations of duskside compressional Pc5 waves

O. D. Constantinescu,[1,2] K.-H. Glassmeier,[1] F. Plaschke,[1] U. Auster,[1] V. Angelopoulos,[3] W. Baumjohann,[4] K.-H. Fornaçon,[1] E. Georgescu,[5] D. Larson,[6] W. Magnes,[4] J. P. McFadden,[6] R. Nakamura,[4] and Y. Narita[1]

Received 20 June 2008; revised 19 April 2009; accepted 14 May 2009; published 14 August 2009.

[1] The five Time History of Events and Macroscale Interactions during Substorms (THEMIS) spacecraft offer new possibilities to analyze ULF waves in the magnetosphere by means of multipoint measurements. During the coast phase, THEMIS observed many compressional oscillations with periods in the Pc5 range and longer. The observed events occur inside a well-defined spatial domain in the outer equatorial duskside magnetosphere. We analyze these waves using the unique string-of-pearls configuration of the THEMIS constellation to evaluate their phase speed and propagation direction. We find that the waves are propagating sunward (westward) and radially outward, orthogonal to the mean magnetic field, with phase speeds around 30 km/s and higher in the spacecraft frame. In the plasma frame the propagation direction is still sunward, with lower speeds (up to 30 km/s for most events). The oscillations exhibit a strong anticorrelation between the magnetic field and the plasma density. On the basis of this, as well as their low propagation speed, orthogonal to the mean magnetic field propagation direction and almost parallel to the magnetic field maximum variance direction, we conclude that the most likely source of these waves is the drift mirror instability.

Citation: Constantinescu, O. D., et al. (2009), THEMIS observations of duskside compressional Pc5 waves, *J. Geophys. Res.*, *114*, A00C25, doi:10.1029/2008JA013519.

1. Introduction

[2] Compressional Pc5 waves [*Anderson*, 1993; *Takahashi et al.*, 1990; *Takahashi*, 1998] have first been observed in space in the late 1960s [*Brown et al.*, 1968; *Sonnerup et al.*, 1969; *Lanzerotti et al.*, 1969]. They predominantly occur in the dusk sector, but also in the dawn [*Vaivads et al.*, 2001; *Rae et al.*, 2007] and, sometimes, in the noon sector [*Takahashi et al.*, 1985]. They have periods between 2 and 10 min in the spacecraft frame [*Jacobs et al.*, 1964] and wave lengths of several R_E [*Walker et al.*, 1982; *Takahashi et al.*, 1985; *Lin et al.*, 1988]. The waves in the duskside are correlated with the development of the partial ring current during storm time [*Barfield and McPherron*, 1972, 1978; *Woch et al.*, 1990]. The direction of propagation for the duskside waves has been determined from multisatellite and radar observations to be westward [*Walker et al.*, 1982; *Takahashi et al.*, 1990; *Lin et al.*, 1988]. Eastward propagation is sometimes observed for the dawnside waves [*Takahashi et al.*, 1990]. The values obtained for the phase speed are between a few km/s and hundred km/s: *Takahashi et al.* [1985] found wave speeds between 4 and 14 km/s using two spacecraft to perform timing analysis. By combining ground and space measurements, *Walker et al.* [1982] found speeds of 32 km/s. *Lin et al.* [1988] based their analysis on the finite Larmor radius effect [*Kivelson and Southwood*, 1983] and reported phase speeds between 33 and 170 km/s.

[3] Much effort has been spent in finding the potential generation mechanism of these waves and several possibilities have been put forward. *Lanzerotti et al.* [1969] advanced the drift mirror instability driven by plasma temperature anisotropy [*Hasegawa*, 1969; *Pokhotelov et al.*, 2003, 2004; *Treumann and Baumjohann*, 1997; *Treumann et al.*, 2004] as the primary generation mechanism for compressional Pc5 waves. As opposed to the classical mirror mode which consists in magnetic structures frozen into the plasma [*Baumjohann and Treumann*, 1996; *Treumann and Baumjohann*, 1997], the magnetic field and density gradients cause the drift mirror mode to slowly propagate with the Larmor drift velocity [*Hasegawa*, 1969]. The drift mirror mode origin is supported by the measured anticorrelation between the plasma pressure and the magnetic field magnitude and by the association of these waves with enhanced plasma β [*Zhu and Kivelson*, 1991, 1994] but

[1]Institut für Geophysik und extraterrestrische Physik, Technische Universität Braunschweig, Braunschweig, Germany.
[2]Institute for Space Sciences, Bucharest, Romania.
[3]Institute of Geophysics and Planetary Physics, University of California, Los Angeles, California, USA.
[4]Institut für Weltraumforschung, Österreichische Akademie der Wissenschaften, Graz, Austria.
[5]Max Planck Institute for Solar System Research, Katlenburg-Lindau, Germany.
[6]Space Sciences Laboratory, University of California, Berkeley, California, USA.

0148-0227/09/2008JA013519$09.00

most of the times the classical mirror instability condition is difficult to be fulfilled. Better agreement is obtained by taking into account the effect of the curvature of the magnetic field which reduces the instability threshold [*Woch et al.*, 1988; *Hasegawa and Chen*, 1989]. However, recently, *Rae et al.* [2007] analyzed an event in the equatorial dawnside magnetosphere for which the linear instability criterion was fully satisfied.

[4] Closely related with the mirror modes are the so-called plasma blobs observed mostly in the morningside of the magnetosphere. They are sunward propagating high β plasma structures, believed to originate in the low-latitude boundary layer in the magnetospheric tail [*Haerendel et al.*, 1999, 2004].

[5] The solar wind triggered Kelvin-Helmholtz instability at the magnetopause or at the low-latitude boundary layer is another possible source for these waves [*Southwood*, 1979; *Fujita et al.*, 1996]. The correlation between the solar wind velocity and the Pc5 pulsations both on the ground and in space [*Engebretson et al.*, 1998] supports this theory. A complication is that most observations show an antisunward propagation which is opposite to what is expected for waves generated at the magnetopause by the solar wind. However, sunward propagating magnetopause surface waves, with azimuthal wavelength close to 4, have been found by *Nielsen* [1984]. The author speculates that changes in the tail configuration are associated with these waves. Another alternative is Kelvin-Helmholtz instability at the interface with sunward convecting flow channels also related with tail processes. Such flow channel excited Kelvin-Helmholtz waves have been reported in the magnetotail, e.g., by *Volwerk et al.* [2007].

[6] An appealing generation mechanism is proposed by *Mager and Klimushkin* [2007]. They show that a wave can be excited by an azimuthally drifting cloud of energetic particles. The resulting wave is propagating in the same direction with the cloud (westward for ions). However, these waves propagate with Alfvén speed, which is higher than the phase speeds measured in other studies.

[7] In this paper we perform a statistical study of compressional Pc5 waves in the outer equatorial duskside magnetosphere using multipoint measurements from Time History of Events and Macroscale Interactions during Substorms (THEMIS) [*Angelopoulos*, 2008] to determine, among other parameters, the phase speed and the propagation direction of the waves. The THEMIS fleet consists of five identical spacecraft flying on equatorial highly elliptical orbits around the Earth. All spacecraft were launched together on February 17, 2007 into identical orbits with apogee at 15.4 R_E in the night-dusk sector (see Figure 1).

[8] In the outer magnetosphere, three spacecraft were grouped at distances of the order of 1000 km, while the remaining two were bracketing this group at distances of the order of 10000 km. These scales are very suitable for the study of Pc5 because the time lags for the wave detection range from seconds, between the three grouped spacecraft, to minutes between the leading and the trailing one. For these time scales there is little change in the wave form; therefore, timing analysis can be performed. During the 7 month coast phase, the apogee slowly rotated from the dusk to the dawn sector, covering the duskside, noonside, and dawnside magnetosphere, enabling a statistical investigation of the waves locations.

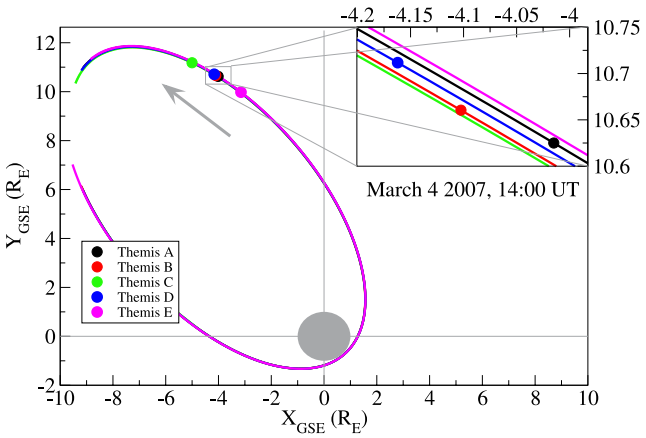

Figure 1. THEMIS orbit two weeks after launch, projected to the GSE equatorial plane. All five spacecraft followed almost the same orbit with the apogee at 15.4 R_E and perigee at 1.07 R_E. The dots represent the spacecraft positions at 1400 UT; the gray arrow shows the direction of motion of the spacecraft along the orbit. The inset shows a zoom on THA, THB, and THD. The distance between spacecraft is much larger than the distance between their orbits.

[9] We use magnetic field data provided by the Flux Gate Magnetometer (FGM) instrument at spin resolution (3 s). This time resolution is more than sufficient for studying pulsations in the Pc5 range. The FGM instrument is similar to the magnetic fields instruments on CLUSTER [*Escoubet et al.*, 1997] and has been described in detail by *Auster et al.* [2008]. The particle data have been obtained from the Electrostatic Analyzers (ESAs) [*McFadden et al.*, 2008] and the Solid State Telescope (SST) (D. Larson, personal communication, 2009). The ESA instrument measures the flux of thermal particles with energies from 3 eV to 25 keV, it provides the 3-D distributions and produces onboard moments for the density, velocity, and temperature of the ambient electrons and ions. The SST instrument is designed to detect particles with energies above the ESA's 25 keV threshold, up to 6 Mev. Since both high- and low-energy particles have a significant contribution for the selected events, we combine measurements from ESA and SST.

[10] To evaluate the phase velocities we use a timing technique which takes advantage of the string-of-pearls configuration of the THEMIS spacecraft to produce accurate results and to eliminate the sign ambiguity in the propagation direction obtained through Minimum Variance Analysis (MVA). We chose one typical event to demonstrate the technique, then we perform a statistical investigation using three months of data.

2. Phase Speed Determination

[11] Between March and May 2007, the maximum distance between the spacecraft orbits was less than 300 km, much smaller than the interspacecraft distances. We can consider that they follow a single common orbit (Figure 1). This string-of-pearls configuration turns the THEMIS fleet

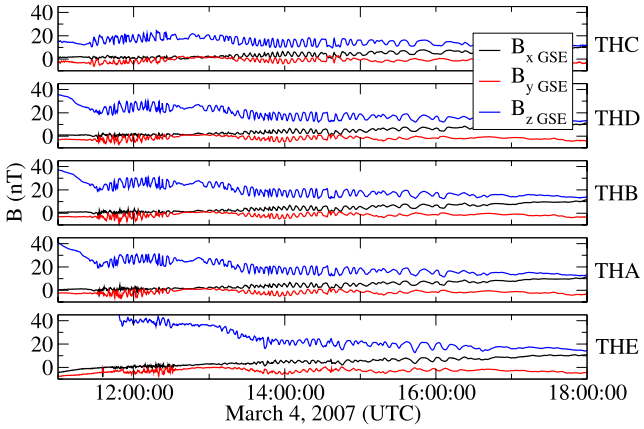

Figure 2. Magnetic field in GSE coordinates measured by THEMIS C, D, B, A, and E (top to bottom, following their order on the common orbit) on 4 March 2007 between 1100 and 1900 UT. Two wave trains are detected by all five spacecraft: first around 1200 UT and second between 1300 and 1600 UT. The second wave train suddenly changes frequency around 1430 UT. For the example presented here we use data approximately between 1330 and 1430 UT.

into a very convenient timing tool. We use this to determine the ULF waves propagation speed along the common orbit. Together with the propagation direction derived from MVA this gives the complete phase velocity vector.

[12] We define the Mean Track Coordinate System (MTCS) as the one dimensional coordinate system given by the position along the average spacecraft orbit. The origin is chosen to be the initial position of the last spacecraft, and the positive direction corresponds to the direction of motion of the spacecraft along the orbit. To determine the propagation speed of the observed waves along the mean track, we cross-correlate the wave forms measured by different spacecraft to obtain the spatial and temporal lags used for the speed calculation. The propagation direction of the wave is given by the minimum variance direction. Using the angle between the mean track and the propagation direction we obtain the phase speed in the spacecraft frame. Providing that plasma data is available, we can transform to the plasma frame by applying a Doppler correction. Note that single spacecraft minimum variance analysis alone can determine the propagation direction only up to a sign. However, the propagation speed along the mean track allows us to lift this indetermination.

[13] To rigorously determine if the detected wave can be locally approximated with a plane wave would require a three dimensional knowledge of the wave field which is not available for the current spacecraft configuration. If such a configuration would be available, a detailed analysis of the wave front curvature would be possible [*Constantinescu et al.*, 2006]. In the present case we can only assume plane waves and near constant phase velocities.

[14] An advantage of using the MTCS is the possibility to quickly check the validity of our assumptions by directly comparing the speeds obtained from different spacecraft pairs. Another advantage is that it provides a direct image of the spatial extent over which the wave was detected.

[15] For each component of the magnetic field, the five THEMIS spacecraft give 10 independent estimates for the wave propagation speed along the orbit. There are also 5 independent estimates for the propagation direction. This greatly improves the accuracy compared with timing techniques involving only two spacecraft.

3. Single Event Analysis

[16] As an example we select an ULF wave detected on March 4 2007 between 1300 and 1500 UT. Figure 2 shows the magnetic field data in GSE coordinates. Two distinct wave trains can be seen as the spacecraft move outward inside the equatorial duskside magnetosphere. The first event has a duration of about one hour around 1200 UT, while the second, with longer duration, follows shortly after.

[17] From Figure 2 it is visible that the frequency of the second wave is not constant but decreases after 1430 UT. This decrease of frequency with the radial distance has been observed previously, e.g., by *Baumjohann et al.* [1987]. In this analysis we concentrate on this later wave train. We chose one hour time interval, around 1400 UT, where the oscillations are nearly sinusoidal. The event has a period close to 5 min and occurs at a radial distance between 10 R_E (THE) and 13 R_E (THC).

[18] The orbits and the spacecraft positions at 1400 UT are shown in Figure 1. THEMIS spacecraft C (THC) is leading the formation followed at about 1.1 R_E distance by THD, THB, and THA which are separated from each other by about 600 km. Around 1.3 R_E behind them, THE closes the formation. In the time domain, the group THD, THB, THA follows THC with a delay of about one hour, while the time separation between the three spacecraft in close proximity is about 5 min. THE passes the same locations one hour later. During the event, the spacecraft cover a distance of about 3.5 R_E along the mean track (from the beginning of the event at THC to the end of the event at THE), each of them detecting the event over a distance of approximately 1.2 R_E.

[19] The detrended, time-windowed data, transformed in field-aligned coordinates and in the MTCS is shown in Figure 3. The $\hat{\mathbf{y}}_{FA}$ unit vector is orthogonal to $\hat{\mathbf{z}}_{FA}$ and to the radial direction vector and points westward. As the origin of the MTCS we choose the initial position of the last spacecraft, THE and the units of length are Earth radii. A first observation is the compressional character of the wave. The z component clearly dominates the transverse components.

[20] The wave travels between the first four spacecraft without any significant change over more than 1 R_E distance. However, THE, which is deeper inside the magnetosphere (though only 1.3 R_E away from THD, THB, and THA), detects a slightly different wave form.

[21] THEMIS E seems to be outside, or at the border of the domain where the wave has constant properties. This leads to poor correlation with the wave forms measured by the other spacecraft; therefore, for the moment we eliminate it from our analysis. However, there still remain 6 pairs of spacecraft for each magnetic field component giving 18 independent values for the wave phase speed along the mean track. A histogram for the obtained values is shown in Figure 4. The large spread is caused by the y component which, being the smallest, has a high noise ratio. However, all other 12 values computed from x and z components are much better grouped together between −94 and −69 km/s

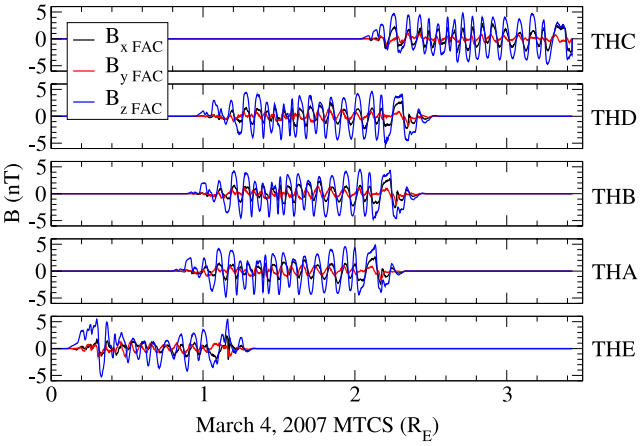

Figure 3. Magnetic field transformed in field-aligned coordinates and MTCS, detrended and windowed on the interval on interest. The z axis is aligned with the mean magnetic field. The y axis, given by the cross product between z direction and the radial direction, points westward. The x axis completes the system. Note how similar the wave forms are for THC, THD, THB, and THA. Also note that because the inferred speed along the orbit is negative, the propagation direction is from right (THC is the first to detect the wave) to left (THE is the last).

(red horizontal line in Figure 4) with an average of −82 km/s. The "−" sign means that the wave propagates in opposite direction to the spacecraft motion. The values for the wave speed along the orbit obtained from the z component, together with the corresponding cross correlations are shown in Table 1. Note the high correlation coefficients and the low scatter in the speed values for the THD, THB and THA spacecraft. There is still a difference between the speeds obtained from the THD, THB, THA group (69–83 km/s) and those obtained from cross correlation between THC and the THD, THB, THA group (85–91 km/s). This suggests that the speed varies along the mean track or the phase fronts are not planar over the distance between THC and the THD, THB, and THA group.

[22] We can now check how well the wave propagated from the other spacecraft fits to the THE data. The distance along the orbit between THA and THE is 7617 km. This corresponds to 92 s for the average speed of −82 km/s. We translate the THA data with this time lag and plot it together with the THE data in Figure 5. While not perfect, the correlation between the waveforms from the two spacecraft confirms the speed we deduced.

[23] The propagation direction (up to a sign) for the wave at each spacecraft can be obtained via MVA. Together with the propagation speed along the orbit this fully determines the wave phase velocity vector in the spacecraft frame: v_{ph} = 36 km/s, θ_{GSE} = 98°, φ_{GSE} = −25°. The wave propagates sunward, orthogonal to the mean local magnetic field ($\widehat{\mathbf{kB}}$ = 89°) and it makes an angle of 116° with the mean local orbit tangent. The associated wave length is about 1.5 R_E. The ratio between the maximum and the minimum eigenvalue of the variance matrix ($\lambda_{max}/\lambda_{min}$) is 19, much larger as the ratio between the intermediate and minimum eigenvalue ($\lambda_{int}/\lambda_{min}$ = 2). This indicates an elongated (cigar-shaped) variance ellipsoid. The low value of $\lambda_{int}/\lambda_{min}$ also means that the uncertainty in determining the propagation direction is relatively high. However, given that the minimum variance direction agrees very well between the five spacecraft (including THE) we are confident that the result reflects at least qualitatively the propagation of the wave: slow, westward, and orthogonal to the magnetic field. The maximum variance direction makes an angle of 22° with the magnetic field, which means that the variance ellipsoid is almost aligned with the magnetic field.

[24] The propagation direction of the wave and the low phase velocity suggest a static magnetic structure convected with the plasma flow. The steepened and nonlinear appearance of the wave, the compressional character, the shape of the variance ellipsoid and its close alignment with the mean magnetic field are all characteristic to mirror modes [*Erdős and Balogh*, 1996; *Lucek et al.*, 1999; *Volwerk et al.*, 2008]. For this particular event, no plasma data is available to apply the Doppler correction to the phase speed or to check the correlation between the magnetic field and the plasma density. However, similar events presented in the next section exhibit very low phase speeds in the plasma frame and anticorrelated oscillations of the magnetic field and plasma density.

4. Statistical Results

[25] We analyze 34 events during the three month when THEMIS was covering the dusk sector (1 March to 30 May 2007). The events are selected by visually inspecting the data for wave trains which clearly stand out from the background field, with frequencies in the Pc5 range, detected by all five spacecraft. For each event we follow the procedure described in section 3 to obtain the phase speed. We request a minimum correlation of 0.7 to allow a spacecraft pair to enter the statistics. Furthermore, in order to increase the accuracy, we consider only the maximum amplitude component of the magnetic field (almost always B_z, the compressional component) which generally shows

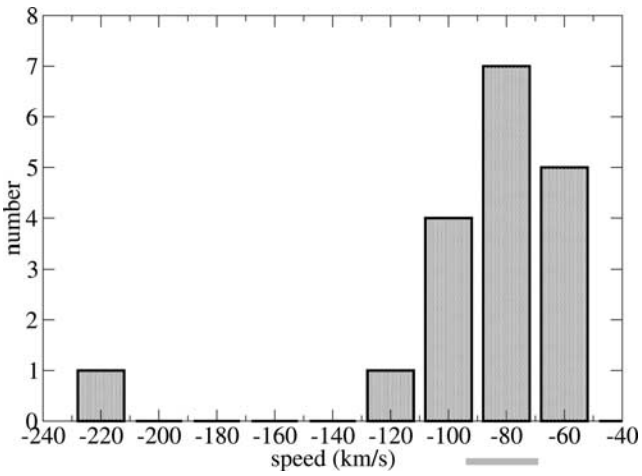

Figure 4. The values for the speed along the mean track, obtained from different spacecraft pairs (without THE), for all components of the magnetic field. The y component causes most of the scatter. The values obtained from x and z components are all within the range marked by the gray horizontal line.

Table 1. Propagation Speeds Along Orbit/Cross-Correlation Coefficients for the Field-Aligned Component z[a]

	THC	THD	THB	THA	THE
THC	-/1.00	**91**/0.86	**90**/0.85	**85**/0.85	-/0.38
THD	91/0.86	-/1.00	**83**/0.99	**76**/0.98	-/0.47
THB	90/0.85	83/0.99	-/1.00	**69**/0.99	-/0.47
THA	85/0.85	76/0.98	69/0.99	-/1.00	-/0.48
THE	-/0.38	-/0.47	-/0.47	-/0.48	-/1.00

[a]Propagation speeds are absolute values. The cross correlations are very high for the first four spacecraft but low for THE. For the propagation speed there are six independent estimations (bold values) which give close values.

better correlation. After applying these restrictions we end up with 139 single spacecraft events corresponding to the 34 ULF waves. For 25 of these waves, low-resolution (6 min) particle data are available from the ESA instrument, allowing for Doppler correction.

[26] Spin resolution (3 s) particle data is available for 22 waves from both ESA and SST instruments. For these waves is possible to obtain the cross-correlation coefficient between the magnetic field intensity and the ion number density which is shown in Figure 6. The degree of anti-correlation displayed by most events suggests that these waves are generated by the mirror mode instability.

[27] In Figure 7 we show statistical results for the selected waves. The measured periods of the waves fall into the Pc5 domain and longer (Figure 7a), most with a period around 5–7 min. The most probable wave length is around 2–3 R_E, but can be larger for long period, fast propagating waves (Figure 7b). The ratio of the variance matrix eigenvalues is shown in Figure 7c. The ratio $\lambda_{max}/\lambda_{min}$ is much larger than $\lambda_{int}/\lambda_{min}$, which means that the variance ellipsoids are cigar-shaped. The relatively low intermediate to minimum eigenvalue ratio (close to 2 for most events) means that the propagation direction in the plane orthogonal to the magnetic field is not very precise determined. However, the consistent westward character of all events suggests that this uncertainty does not severely influences our results. The blue bars in Figure 7d represent the angle between the maximum variance direction and the mean magnetic field. This is within 30° for most events, indicating that the variance ellipsoids are aligned almost parallel with the magnetic field. Following *Erdős and Balogh* [1996] and *Lucek et al.* [1999], this is a strong indication of mirror mode activity. The gray bars in Figure 7d show that propagation orthogonal to the magnetic field is clearly favored, with all waves propagating within 30° from the direction orthogonal to the magnetic field. This makes the slow mode (which also exhibits anticorrelation between the magnetic field and the particle density, and low phase speeds) an improbable candidate for the observed waves. Furthermore, the slow mode is strongly damped owing to wave-particle interactions.

[28] For the 25 events for which plasma flow velocity (ESA ion bulk velocity) was available we apply a Doppler correction. The Doppler factor for these events, $1 - (v_{flow}/v_{phase}^{sc\ \ frame})\cos(\alpha)$, is shown in Figure 7e. Its value is between 0 and 1 for most events, meaning that in the plasma frame the waves are propagating with lower speeds than measured in the spacecraft frame. The positive value also means that the propagation direction in the plasma frame remains the same as the propagation direction in the spacecraft frame (velocity does not change sign when the Doppler correction is applied). The gray bars in Figure 7f stand for the propagation speed along the orbit obtained through correlation analysis (absolute value). For most of the events this falls between 20 and 100 km/s. The red bars are for the phase speed in the spacecraft frame after taking into account the propagation direction from MVA. The values have a smaller spread with most of them up to 50 km/s. The Doppler corrected phase speed (absolute value) is represented with the blue bars. For most of the events the phase speed in the plasma frame is lower than 30 km/s which confirms once more the drift mirror mode nature of these waves.

[29] The propagation directions in the spacecraft frame, which is the same with the propagation direction in the plasma frame for most of the detected waves, can be seen in Figure 8. We choose a field-aligned coordinate system with the z axis along the main magnetic field. The y axis is given

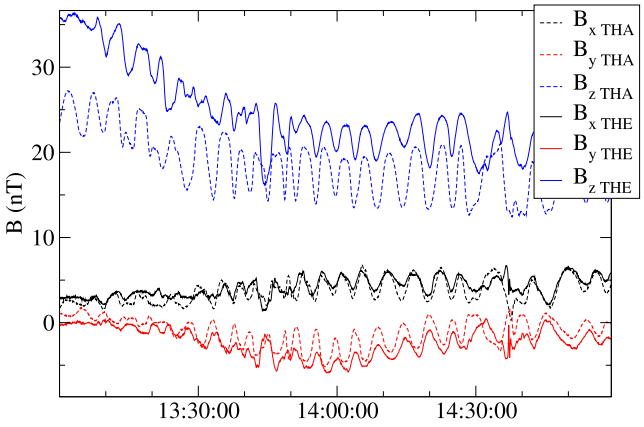

Figure 5. Comparison between the waveforms measured by THE (solid line) and the THA (dashed line) data translated with a time lag of 92 s, corresponding to a phase speed of −82 km/s. GSE coordinates.

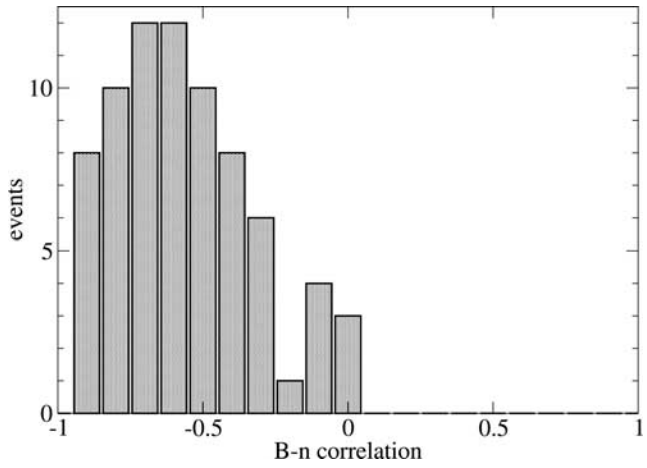

Figure 6. Cross correlation between the magnetic field magnitude and the ion number density (74 single spacecraft events). Most events show that the magnetic field was oscillating in anti-phase with the plasma density. The density was obtained by combining ESA and SST plasma data. The magnetic field was measured by the FGM instrument.

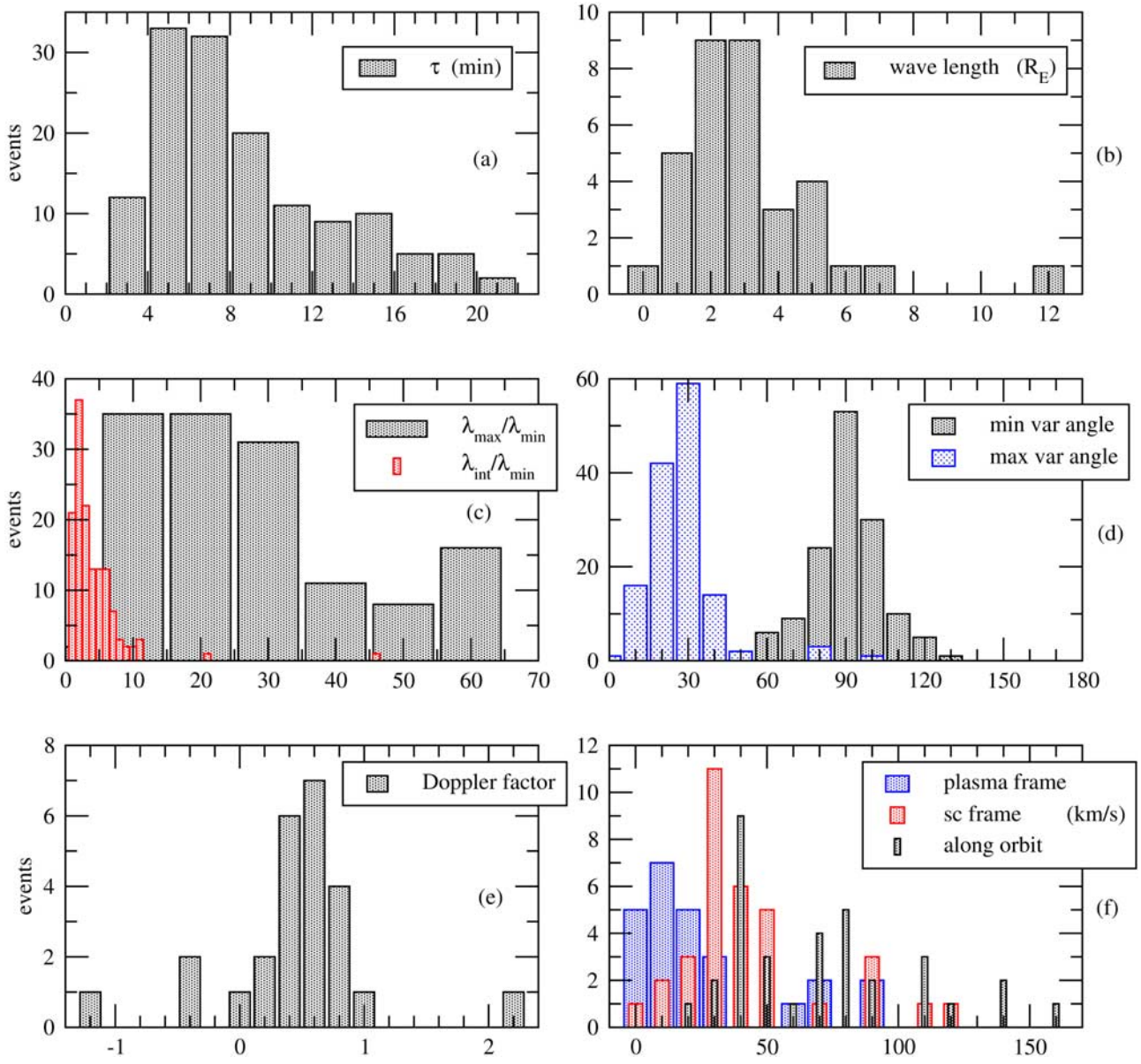

Figure 7. Statistical results. (a) The wave period. It falls into Pc5 and longer range with most events close to 5 min (138 single spacecraft events). (b) The wave length. Most of the times 2 to 3 R_E (34 waves). (c) Variance matrix eigenvalue ratios. The maximum to minimum ratio is much larger than the intermediate to minimum ratio; therefore, the variance ellipsoid is cigar-shaped (138 single spacecraft events). (d) Gray indicates the angle between the propagation direction and the local mean magnetic field. The orthogonal character of the waves is evident. Blue indicates the angle between the maximum variance direction and the local mean magnetic field. Most of the times under 30°; structures are aligned with the magnetic field (138 single spacecraft events). (e) The Doppler factor. It is positive for most events; therefore, the Doppler correction does not change the sign of the phase velocity. Note the lower than unity absolute value for the majority of the events (25 waves). (f) Propagation speeds. Gray, speed along orbit (34 waves); red, phase speed in the spacecraft frame (34 waves); blue, phase speed in the plasma frame (25 waves).

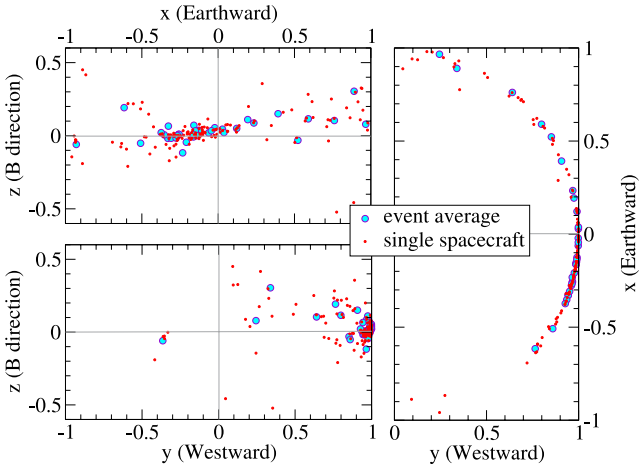

Figure 8. Waves propagation directions (projection of phase velocity unit vector) in local field-aligned coordinates. The z axis is parallel with the mean magnetic field. The y axis points westward and is orthogonal to the direction to the Earth. The x axis completes the system, pointing approximately toward Earth. The red dots represent single spacecraft propagation directions; blue circles represent event averages. The waves propagate orthogonal to the magnetic field, westward (sunward), and slightly away from the Earth, toward the magnetopause.

by the cross product between $\hat{\mathbf{z}}$ and the geocentric position vector. In our case (close to equatorial plane, duskside magnetosphere) the direction of the y axis is very close to westward direction. The x axis completes the system, pointing approximately toward Earth for the events studied here. The red dots are the MVA results from single spacecraft and the blue circles are the directions after averaging over each wave event. The predominantly westward propagation in the spacecraft frame appears clearly from this picture. For only one event the wave was propagating in the opposite direction. For all but three of the waves, the propagation direction remains sunward also in the plasma frame after applying the Doppler correction. The orthogonal character of the waves can be easily seen in Figure 8. Because of this, the waves tend to remain confined close to the magnetic equatorial plane. The majority of the dots have a negative x coordinate. This indicate propagation away from the Earth, toward the magnetopause.

[30] The locations and phase velocities of the detected wave trains are depicted in Figure 9. Here, the dotted gray lines are the first and last spacecraft orbits considered in this study, based on the presence of waves in the data set. The black solid lines show the spacecraft orbit segments during the detection time. The phase speed is represented by the blue circles. The radii of the circles are proportional with the phase speed. The red arrows are the projections of the phase speed unit vectors on the $(x, y)_{GSE}$ plane. We have not found clear wave trains in the dusk sector after May 30 2007. This last orbit is the domain boundary in sunward direction. Because of the lack of data before March 2007, the anti-sunward boundary is uncertain. In the radial direction the domain extends from about 8 R_E up to the magnetopause. The phase velocity is directed westward and its magnitude seems to be higher in the center of the domain and to decrease toward the boundaries.

[31] We note here the very good agreement between the spatial domain we determine for these waves and the location of the magnetospheric (MSP) population described by *Claudepierre et al.* [2008]. These waves, with frequencies in the range of 0.5 to 3 mHz, appear in their global MHD simulation both in the dusk and the dawn sectors.

5. Summary and Conclusions

[32] In this paper we have investigated from a statistical point of view, duskside compressional Pc5 waves detected by the THEMIS spacecraft during three months. We took advantage on the string-of-pearls configuration of the THEMIS fleet to derive the phase velocity of the waves by combining a timing technique with minimum variance analysis.

[33] Because of the fact that in this early stage of the mission, the particle instruments were not fully operational, we were not able to compute the phase speed in the plasma frame and the correlation between the magnetic field and the plasma density for one third of the studied waves. However, for most of the remaining two thirds, we found that the magnetic field oscillates in antiphase with the plasma density and also that the phase speed of the waves is very low in the plasma frame (under 30 km/s for most of them), orthogonal to the magnetic field. This suggest they are drift mirror waves. In favor of this interpretation are also the variance ellipsoids associated with these structures. They are cigar-shaped and elongated parallel to the mean magnetic field, as expected for mirror structures.

[34] We found that the waves are located in the outer equatorial magnetosphere at a radial distance larger than 8 R_E, up to the magnetopause, and they do not penetrate more than 5 R_E in the x_{GSE} direction. Most of them have wave lengths between 2 and 3 R_E, and they propagate orthogonal to the background magnetic field, in westward direction both in the spacecraft and in the plasma frame. This propagation direction is consistent with drift mirror waves which propagate with the Larmor drift velocity.

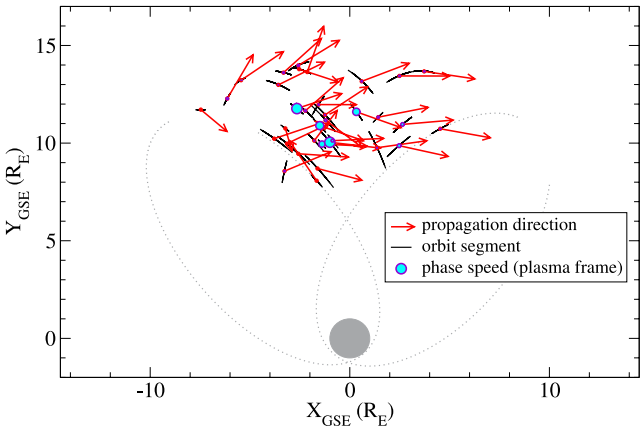

Figure 9. Locations and phase velocities. Sun is to the right. The gray dotted lines are the THEMIS orbits for the first and last events. The black solid lines indicate the locations of the detected waves. The radii of the blue circles are proportional with the phase speeds. The red arrows are projections of the phase velocities on the $(x, y)_{GSE}$ plane (arbitrary units).

[35] **Acknowledgments.** One of the authors (O.D.C.) is grateful to M. Connors, S. R. Elkington, S. G. Claudepierre, and I. Mann for thoughtful discussions and suggestions. The IGeP team was financially supported by the German Zentrum für Luft und Raumfahrt under grant 50QP0402. THEMIS is supported in the United States by NASA NAS5-02099.

[36] Zuyin Pu thanks Oleg Pokhotelov, I. Rae, and another reviewer for their assistance in evaluating this paper.

References

Anderson, B. J. (1993), Statistical studies of Pc 3–5 pulsations and their relevance for possible source mechanisms of ULF waves, *Ann. Geophys.*, *11*, 128–143.

Angelopoulos, V. (2008), The THEMIS mission, *Space Sci. Rev.*, *141*, 5–43.

Auster, H. U., et al. (2008), The THEMIS fluxgate magnetometer, *Space Sci. Rev.*, *141*, 235–264.

Barfield, J. N., and R. L. McPherron (1972), Statistical characteristics of storm-associated pc 5 magnetic micropulsations observed at synchronous equatorial orbit, *J. Geophys. Res.*, *77*, 4720–4733.

Barfield, J. N., and R. L. McPherron (1978), Stormtime pc 5 magnetic pulsations observed at synchronous orbit and their correlation with the partial ring current, *J. Geophys. Res.*, *83*, 739–743.

Baumjohann, W., and R. A. Treumann (1996), *Basic Space Plasma Physics*, Imperial Coll. Press, London.

Baumjohann, W., N. Sckopke, J. LaBelle, B. Klecker, H. Luehr, and K. H. Glassmeier (1987), Plasma and field observations of a compressional Pc 5 wave event, *J. Geophys. Res.*, *92*, 12,203–12,212.

Brown, W. L., L. J. Cahill, L. R. Davis, C. S. McIlwain, and C. E. Roberts (1968), Acceleration of trapped particles during a magnetic storm on April 18, 1965, *J. Geophys. Res.*, *73*, 153–161.

Claudepierre, S. G., S. R. Elkington, and M. Wiltberger (2008), Solar wind driving of magnetospheric ULF waves: Pulsations driven by velocity shear at the magnetopause, *J. Geophys. Res.*, *113*, A05218, doi:10.1029/2007JA012890.

Constantinescu, O. D., K.-H. Glassmeier, U. Motschmann, R. A. Treumann, K.-H. Fornaçon, and M. Fränz (2006), Plasma wave source location using CLUSTER as a spherical wave telescope, *J. Geophys. Res.*, *111*, A09221, doi:10.1029/2005JA011550.

Engebretson, M., K.-H. Glassmeier, M. Stellmacher, W. J. Hughes, and H. Lühr (1998), The dependence of high-latitude Pc5 wave power on solar wind velocity and on the phase of high-speed solar wind streams, *J. Geophys. Res.*, *103*, 26,271–26,384.

Erdős, G., and A. Balogh (1996), Statistical properties of mirror mode structures observed by Ulysses in the magnetosheath of Jupiter, *J. Geophys. Res.*, *101*, 1–12.

Escoubet, C. P., R. Schmidt, and M. L. Goldstein (1997), Cluster: Science and mission overview, *Space Sci. Rev.*, *79*, 11–32.

Fujita, S., K. H. Glassmeier, and K. Kamide (1996), MHD waves generated by the Kelvin-Helmholtz instability in a nonuniform magnetosphere, *J. Geophys. Res.*, *101*, 27,317–27,326.

Haerendel, G., et al. (1999), High-beta plasma blobs in the morningside plasma sheet, *Ann. Geophys.*, *17*, 1592–1601.

Haerendel, G., E. Georgescu, K. Glassmeier, B. Klecker, Y. Bogdanova, H. Rème, and H. Frey (2004), Cluster observes formation of high-beta plasma blobs, *Ann. Geophys.*, *22*, 2391–2401.

Hasegawa, A. (1969), Drift mirror instability in the magnetosphere, *Phys. Fluids*, *12*, 2642.

Hasegawa, A., and L. Chen (1989), Theory of the drift mirror instability, in *Plasma Waves and Instabilities at Comets and in Magnetospheres*, *Geophys. Monogr. Ser.*, vol. 53, edited by B. T. Tsurutani and H. Oya, pp. 173–177, AGU, Washington, D. C.

Jacobs, J. A., Y. Kato, S. Matsushita, and V. A. Troitskaya (1964), Classification of geomagnetic micropulsations, *J. Geophys. Res.*, *69*, 180–181.

Kivelson, M. G., and D. J. Southwood (1983), Charged particle behavior in low-frequency geomagnetic pulsations: 3. Spin phase dependence, *J. Geophys. Res.*, *88*, 174–182.

Lanzerotti, L. J., A. Hasegawa, and C. G. MacLennan (1969), Drift mirror instability in the magnetosphere: Particle and field oscillations and electron heating, *J. Geophys. Res.*, *74*, 5565–5578.

Lin, N., R. L. McPherron, M. G. Kivelson, and D. J. Williams (1988), An unambiguous determination of the propagation of a compressional Pc 5 wave, *J. Geophys. Res.*, *93*, 5601–5612.

Lucek, E. A., M. W. Dunlop, A. Balogh, P. Cargill, W. Baumjohann, E. Georgescu, G. Haerendel, and K.-H. Fornaçon (1999), Identification of magnetosheath mirror modes in Equator-S magnetic field data, *Ann. Geophys.*, *17*, 1560–1573.

Mager, P. N., and D. Y. Klimushkin (2007), Generation of Alfvén waves by a plasma inhomogeneity moving in the Earth's magnetosphere, *Plasma Phys. Rep.*, *33*, 391–398.

McFadden, J. P., C. W. Carlson, D. Larson, M. Ludlam, R. Abiad, B. Elliott, P. Turin, M. Marckwordt, and V. Angelopoulos (2008), The THEMIS ESA Plasma Instrument and in-flight calibration, *Space Sci. Rev.*, *141*, 277–302.

Nielsen, E. (1984), Observations of sunward propagating waves on the magnetopause, *J. Geophys. Res.*, *89*, 9095–9099.

Pokhotelov, O. A., I. Sandberg, R. Z. Sagdeev, R. A. Treumann, O. G. Onishchenko, M. A. Balikhin, and V. P. Pavlenko (2003), Slow drift mirror modes in finite electron-temperature plasma: Hydrodynamic and kinetic drift mirror instabilities, *J. Geophys. Res.*, *108*(A3), 1098, doi:10.1029/2002JA009651.

Pokhotelov, O. A., R. Z. Sagdeev, M. A. Balikhin, and R. A. Treumann (2004), Mirror instability at finite ion-Larmor radius wavelengths, *J. Geophys. Res.*, *109*, A09213, doi:10.1029/2004JA010568.

Rae, I. J., I. R. Mann, C. E. J. Watt, L. M. Kistler, and W. Baumjohann (2007), Equator-S observations of drift mirror mode waves in the dawnside magnetosphere, *J. Geophys. Res.*, *112*, A11203, doi:10.1029/2006JA012064.

Sonnerup, B. U. Ö., L. J. Cahill Jr., and L. R. Davis (1969), Resonant vibration of the magnetosphere observed from Explorer 26, *J. Geophys. Res.*, *74*, 2276–2288.

Southwood, D. J. (1979), Magnetopause Kelvin-Helmholtz instability, in *Magnetospheric Boundary Layers*, edited by J. Lemaire, *ESA Spec. Publ./, ESA SP-148*357–364.

Takahashi, K. (1998), ULF waves: 1997 IAGA division 3 reporter review, *Ann. Geophys.*, *16*, 787–803.

Takahashi, K., P. R. Higbie, and D. N. Baker (1985), Azimuthal propagation and frequency characteristic of compressional Pc 5 waves observed at geostationary orbit, *J. Geophys. Res.*, *90*, 1473–1485.

Takahashi, K., R. W. McEntire, C. Z. Cheng, and L. M. Kistler (1990), Observation and theory of Pc 5 waves with harmonically related transverse and compressional components, *J. Geophys. Res.*, *95*, 977–989.

Treumann, R. A., and W. Baumjohann (1997), *Advanced Space Plasma Physics*, Imperial Coll. Press, London.

Treumann, R. A., C. H. Jaroschek, O. D. Constantinescu, R. Nakamura, O. A. Pokhotelov, and E. Georgescu (2004), The strange physics of low frequency mirror mode turbulence in the high temperature plasma of the magnetosheath, *Nonlinear Processes Geophys.*, *11*, 647–657.

Vaivads, A., et al. (2001), Compressional Pc5 type pulsations in the morningside plasma sheet, *Ann. Geophys.*, *19*, 311–320.

Volwerk, M., K.-H. Glassmeier, R. Nakamura, T. Takada, W. Baumjohann, B. Klecker, H. Rème, T. L. Zhang, E. Lucek, and C. M. Carr (2007), Flow burst-induced Kelvin-Helmholtz waves in the terrestrial magnetotail, *Geophys. Res. Lett.*, *34*, L10102, doi:10.1029/2007GL029459.

Volwerk, M., T. L. Zhang, M. Delva, Z. Vörös, W. Baumjohann, and K.-H. Glassmeier (2008), First identification of mirror mode waves in Venus' magnetosheath?, *Geophys. Res. Lett.*, *35*, L12204, doi:10.1029/2008GL033621.

Walker, A. D. M., R. A. Greenwald, A. Korth, and G. Kremser (1982), Stare and GEOS 2 observations of a storm time Pc 5 ULF pulsation, *J. Geophys. Res.*, *87*, 9135–9146.

Woch, J., G. Kremser, A. Korth, O. A. Pokhotelov, V. A. Pilipenko, Y. M. Nezlina, and E. Amata (1988), Curvature-driven drift mirror instability in the magnetosphere, *Planet. Space Sci.*, *36*, 383–393.

Woch, J., G. Kremser, and A. Korth (1990), A comprehensive investigation of compressional ULF waves observed in the ring current, *J. Geophys. Res.*, *95*, 15,113–15,132.

Zhu, X., and M. G. Kivelson (1991), Compressional ULF waves in the outer magnetosphere: 1. Statistical study, *J. Geophys. Res.*, *96*, 19,451–19,467.

Zhu, X., and M. G. Kivelson (1994), Compressional ULF waves in the outer magnetosphere: 2. A case study of Pc 5 type wave activity, *J. Geophys. Res.*, *99*, 241–252.

V. Angelopoulos, Institute of Geophysics and Planetary Physics, University of California, Box 951567, 2712 Geology Building, Los Angeles, CA 90095-1567, USA.

U. Auster, O. D. Constantinescu, K.-H. Fornaçon, K.-H. Glassmeier, Y. Narita, and F. Plaschke, Institut für Geophysik und extraterrestrische Physik, Technische Universität Braunschweig, Mendelssohnstrasse 3, D-38106 Braunschweig, Germany. (d.constantinescu@tu-bs.de)

W. Baumjohann, W. Magnes, and R. Nakamura, Institut für Weltraumforschung, Österreichische Akademie der Wissenschaften, Schmiedlstraße 6, A-8042 Graz, Austria.

E. Georgescu, Max-Planck-Institut für Sonnensystemforschung, Max-Planck-Strasse 2, D-37191, Katlenburg-Lindau, Germany.

D. Larson and J. P. McFadden, Space Sciences Laboratory, University of California, 7 Gauss Way, Berkeley, CA 94720-7450, USA.